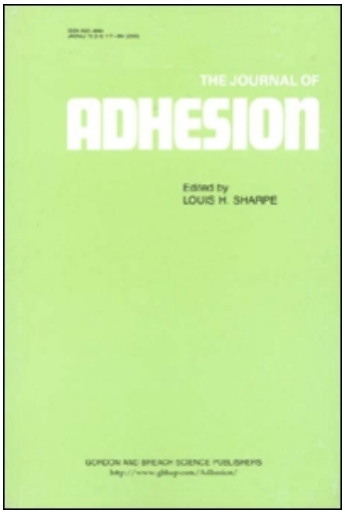

The Journal of Adhesion
Publication details, including instructions for authors and subscription information:
http://www.informaworld.com/smpp/title~content=t713453635

Finite Element Analysis of Thickness Dependent Debonding Forces of Elastomer Coatings

Chung-Souk Han[a]; Chao Zhang[b]; Jialai Wang[b]; Jongsoo Kim[c]; Seok-Bong Choi[c]
[a] Department of Civil Engineering, North Dakota State University, Fargo, North Dakota, USA [b] Department of Civil, Construction, and Environmental Engineering, University of Alabama, Tuscaloosa, Alabama, USA [c] Center for Nanoscale Science and Engineering, North Dakota State University, Fargo, North Dakota, USA

To cite this Article Han, Chung-Souk , Zhang, Chao , Wang, Jialai , Kim, Jongsoo and Choi, Seok-Bong(2007) 'Finite Element Analysis of Thickness Dependent Debonding Forces of Elastomer Coatings', The Journal of Adhesion, 83: 6, 535 — 551
To link to this Article: DOI: 10.1080/00218460701453510
URL: http://dx.doi.org/10.1080/00218460701453510

The Journal of Adhesion, 83:535–551, 2007

ISSN: 0021-8464 print/1545-5823 online
DOI: 10.1080/00218460701453510

Taylor & Francis
Taylor & Francis Group

Finite Element Analysis of Thickness Dependent Debonding Forces of Elastomer Coatings

Chung-Souk Han
Department of Civil Engineering, North Dakota State University, Fargo, North Dakota, USA

Chao Zhang
Jialai Wang
Department of Civil, Construction, and Environmental Engineering, University of Alabama, Tuscaloosa, Alabama, USA

Jongsoo Kim
Seok-Bong Choi
Center for Nanoscale Science and Engineering, North Dakota State University, Fargo, North Dakota, USA

Adhesion tests consisting of cylindrical studs to be pulled off from a soft elastomer coating on a substrate have been widely performed in the literature to characterize various biofouling and adhesive situations. These experiments have shown that the pull-off forces are strongly dependent on the coating thickness. To understand this thickness dependence on the debonding forces, a detailed analysis is performed by the finite element method, applying the virtual crack closure technique. In these simulations, coating thickness, elastic modulus, and initial geometries have been varied to study their influence on the debonding forces. The effect of these factors on the debonding forces is discussed with respect to experimental pull-off results of silicone coatings.

Keywords: Adhesion; Coatings; Debonding; Elasticity; Fracture

INTRODUCTION

To study detachment mechanisms of various biofoulants and other adhesive situations, pull-off tests have been widely performed in the

Received 20 November 2006; in final form 28 March 2007.
Address correspondence to Chung-Souk Han, North Dakota State University, Department of Civil Engineering, 1410 North 14th Avenue (CIE 201), ND 58105, Fargo. E-mail: chung-souk.han@ndsu.edu

literature (see, *e.g.*, Refs. [1–3] and the references therein). In these pull-off experiments, rigid, cylindrical studs are attached to a coating that is strongly bound to a substrate, and the forces required to pull the stud from the coating are measured in an experimental fixture. These experiments have shown that the pull-off forces are strongly dependent on the coating thickness. Analytical predictions applying linear elastic material behavior and fracture mechanics have been derived (*e.g.*, Ref. [4]), which may be able to explain such behavior. Because of simplifying assumptions and idealized geometry, these analytical solutions have some limitations, particularly for thin coatings and small crack lengths [5,6]. To obtain a more detailed analysis, pull-off tests have been performed and the corresponding debonding forces are simulated here by the finite element (FE) method. Such FE simulations have also been performed for the debonding analysis of different material systems in Refs. [7–11] among others.

In this article, pull-off tests composed of aluminum studs attached by an epoxy adhesive to a silicone rubber coating are presented and analyzed by FE simulations. In the following, sample preparation and experimental fixtures of the pull-off tests are described, which are modeled by the FE method applying the virtual crack closure technique. The results of experiments and simulations are subsequently analyzed and discussed.

EXPERIMENTAL

Experimental Setup

A customized adhesion tester was developed to measure adhesion force and displacement at a constant speed (Figure 1). A silicone coating on a glass substrate with three aluminum studs was securely positioned in a sample holder, and then a pull-off gripper was slowly moved into the aluminum stud by the x-axis actuator (LTA-HS, Newport Corporation, Irvine, CA). A universal joint was inserted between the gripper and the load cell (AL311, Honeywell, Columbus, OH) to achieve an improved vertical alignment. The load cell was directly connected to the z-axis actuator (LTA-HL, Newport Corporation, Irvine, CA), and all the actuators were remotely controlled using ESP300 motion-control software (three-axis control, Newport Corporation, Irvine, CA). A position sensor (GHSA 750–250, Macrosensors Inc., Pennsauken, NJ) was fixed to a mount to measure the displacements. As the gripper pulled up the stud at a constant speed ($2\,\mu m/s$), force and displacement data were collected by data acquisition software (LabView 7) until the stud was completely detached

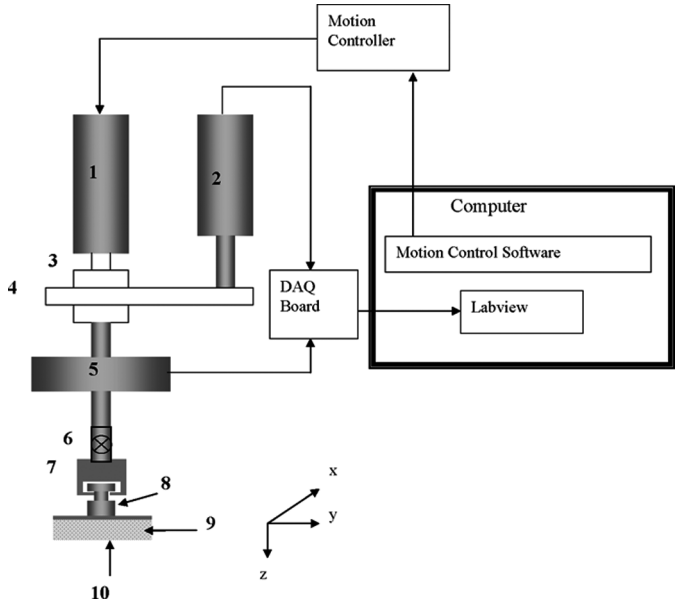

FIGURE 1 Experimental setup for pull-off tests: 1—actuator, 2—linear variable differential transformer, 3—joint, 4—mount, 5—load cell, 6—swivel, 7—gripper, 8—aluminum stud, 9—silicone coating, and 10—$1 \times 3''$ (25.4×76.2 mm) glass slide.

from the coating. After the adhesion test, the contact area of the detached stud was calculated by a digital caliper, and maximum tensile stress values were determined by dividing a maximum tensile force by the related contact area.

Preparation of Silicone Coating

In this research, two different silicone coatings were tested: vinyl-and methacryloxypropyl-terminated polydimethylsiloxane (SP1) and vinyl-terminated polydimethylsiloxane (SC6). These silicone coatings are similarly produced, differing mainly in the ingredients in the manufacturing process. A more detailed description of the silicone-coating production is given in the following.

SP1 (Vinyl and Methacryloxypropyl-Terminated Polydimethylsiloxane)

Methacrylpropyl-terminated polydimethylsiloxane (30 g), of vinyl-terminated polydimethylsiloxane, and 0.2 g of trimethyl-siloxy-terminated vinylmethylsiloxane-dimethylsiloxane copolymers (all from Gelest,

Morrisville, PA) were poured with a syringe into a polypropylene specimen cup. MQ vinyl resins in xylene (10 g, Clariant Corporation, Charlotte, NC) were added with a pipette, and the whole aggregate was mechanically mixed by a stainless steel coiled stir rod attached to a Tallboys stirrer for a couple of minutes. Sixteen drops of Karstedt's catalyst (Gelest, Morrisville, PA) were added to the mixture with a pipette, and the mixture was allowed to blend for an additional 10 min. While mixing, hexamethyldisiloxane-treated silicon dioxide, amorphous (Dow Corning Corporation, Midland, MI), was slowly added with a spatula. Fifteen grams were added this way, intermittently, over a period of about an hour. The mixture was allowed to blend for an additional hour and then refrigerated.

SC6 (Vinyl-Terminated Polydimethylsiloxane)

Vinyl-terminated polydimethylsiloxane (37.5 g), 37.5 g of vinyl-terminated polydimethylsiloxane, and 0.25 g of trimethylsiloxy-terminated vinylmethyl-siloxane-dimethylsiloxane copolymer (all from Gelest, Morrisville, PA) were poured with a syringe into a polypropylene specimen cup. MQ vinyl resins in xylene (12.5 g, Clariant Corporation, Charlotte, NC) were added with a pipette, and the whole aggregate was mechanically mixed by a stainless steel coiled stir rod attached to a Tallboys stirrer for a couple of minutes. Twenty drops of Karstedt's catalyst (Gelest, Morrisville, PA) were added to the mixture and allowed to blend for an additional 10 min. While mixing, hexamethyl-disiloxane-treated silicon dioxide, amorphous (Dow Corning Corporation, Midland, MI), was slowly added. Over a period of about an hour, 18.75 g were added this way, intermittently. The mixture was allowed to blend for an additional hour.

Each of the coating resins was put in a vacuum oven for approximately 3 min to remove any bubbles. The coating solution was then applied on $1 \times 3''$ (25.4×76.2 mm) glass slides and cured at room temperature for more than 3 days.

Determination of Thickness-Dependent Debonding Forces

An aluminum stud was glued on this silicone rubber coating with an epoxy adhesive (see Figure 2), and the displacements and forces were monitored during testing by the pull-off device for various coating thicknesses. The corresponding pull-off forces of various samples are plotted in Figure 3. They show a large increase in the debonding (tensile) stress with decreasing coating thickness. Although there is some scatter in the experimental values, a fit by $y = at^{-b}$, where

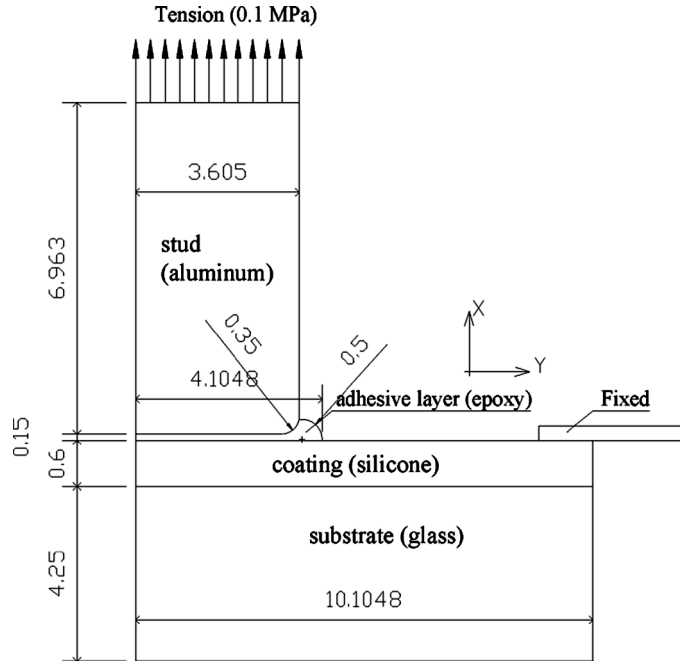

FIGURE 2 Geometry (dimensions in mm) and material configuration.

t denotes the coating thickness, yields reasonable approximations. For both coating samples, however, the fitting parameters a and b vary quite strongly (Figure 3).

DETERMINATION OF THE ENERGY-RELEASE RATE WITH FINITE ELEMENTS

The determination of the energy-release rate with the FE method is quite well established and has been thoroughly discussed in the literature. In the following, the virtual crack closure technique is briefly reviewed. For a review, the interested reader is referred to Krueger [12] and the references therein. It may also be noteworthy that a different pull-off test has also been analyzed with FE in Sun *et al.* [13]. However, the problem considered therein is, related to the debonding of the coating from the substrate.

The relevant FE relation for a bilinear FE can be stated by

$$\frac{1}{4}\sum_{l=1}^{4}[B]_l^T[\sigma]_l V_k = [F]_m, \tag{1}$$

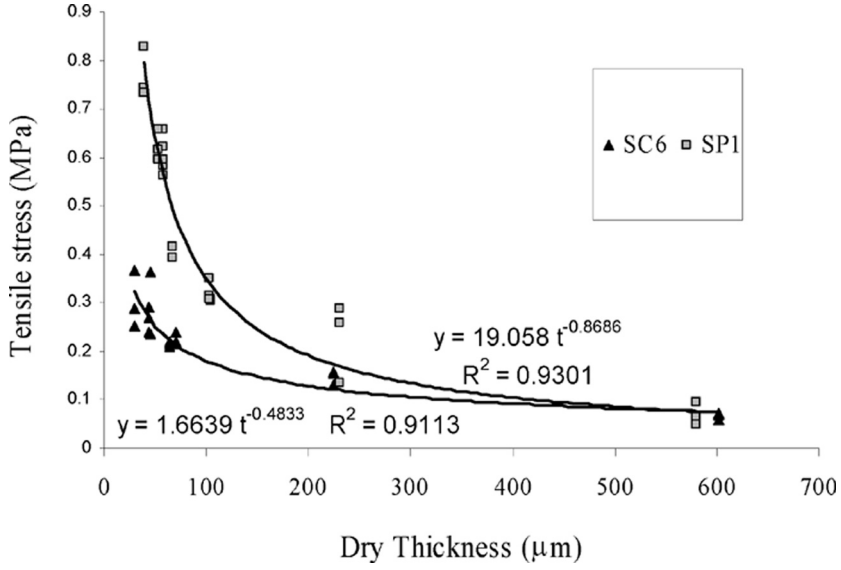

FIGURE 3 Experimentally determined debonding forces (pull-off forces) and fitted curves.

where $[B]$ is the traditionally defined B-matrix with the index, l, denoting the number of integration points and m the number of nodes; $[\sigma]$ represents a column matrix containing the components of the stress tensor, and $V_k = 2\pi R_k A_k$ corresponds to the volume of element k. On the right-hand side, $[F]_m = [F_{z1} \;\; F_{r1} \;\; F_{z2} \;\; F_{r2} \;\; F_{z3} \;\; F_{r3} \;\; F_{z4} \;\; F_{r4}]^T$ contains the nodal forces at the four nodes of the FE (see, *e.g.*, Ref. [14]), where the indices refer to the node numbers and *r, z* to the radial and vertical direction of the nodal force, respectively. The corresponding opening mode, G_I, and shearing mode, G_{II}, components of the energy-release rate can be obtained by

$$G_I = \frac{1}{2\Delta A} F_{zi} \Delta u_j, \qquad G_{II} = \frac{1}{2\Delta A} F_{ri} \Delta v_j, \tag{2}$$

where $\Delta A = \pi(r_1^2 - r_2^2)$ is the crack-opening surface, F_{zi} and F_{ri} respectively refer to the nodal forces at crack tip node i in the vertical and horizontal directions, and $\Delta u_j = u_j - u_{j^*}, \Delta v_j = v_j - v_{j^*}$ are the opening and shearing displacements respectively at node j in the vertical and horizontal directions as shown in Figure 4. The actual energy-release rate (or total energy-release rate) is then obtained by

$$G_t = G_I + G_{II}, \tag{3}$$

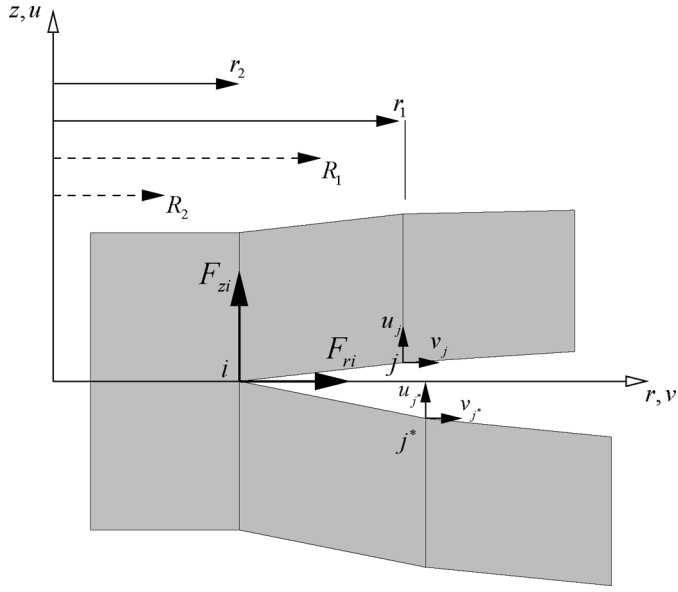

FIGURE 4 Virtual crack closure technique for four-node element.

which is applied to analyze the thickness-dependent debonding forces observed in the pull-off experiments (Figure 3).

SIMULATION RESULTS

The FE results presented in this article were obtained using the general-purpose FE program Marc (MSC Software, Inc., Santa Ana, CA). The geometric and material properties of the specimen, adhesive layer, the coating layer, and the substrate are given in Table 1. The determination of the Young's modulus for the silicone coating is somewhat difficult as it is a quite soft material. When traditional tensile tests are performed, the silicone material can deform because of gravity forces before the specimen is actually elongated. The material properties are also very sensitive to the chemical composition and production process. As the obtained data appeared to be unreliable, four different values (see Table 1) were applied for the Young's modulus in the simulations to study their influence on the simulation results. In the simulations, a uniform tensile stress of $\sigma_o = 0.1\,\text{MPa}$ is assumed at the top, corresponding to a force of about 4 N.

A four-node quadrilateral solid axisymmetric element was applied to model the specimen bonded to the substrate, where the x-axis is

TABLE 1 Material Properties

Components	Young's modulus (MPa)	Poisson's ratio
Specimen(Al)	85,000	0.35
Adhesive (epoxy)	21,500	0.35
Coating (silicone)	0.4, 0.8, 1.4, 10	0.48
Substrate (glass)	69,000	0.22

the rotational and vertical axis. Only half of the specimen has been modeled, due to the axial symmetry, with a particularly fine mesh at the material interfaces (see Figure 5), where an enlarged section of the adaptively discretized FE mesh is shown, along with an arrow indicating the critical location where the debonding was observed in the experiments. The same location was assumed in the determination of the energy-release rates, to be discussed later.

Based on the approach in section 3 the energy-release rate was determined for various thicknesses, t, in a range of 0.05 mm to 0.6 mm. It is assumed that a small crack is initially present in the critical area (indicated by the solid arrow in Figure 5). Such initial cracks are more or less unavoidable as the pull-off specimens have to be handled during test preparations and as very high local stresses (see Figure 6) have to be expected at even small loads because of the geometry. The corresponding strains are quite small and are shown in Figure 7. Besides handling, these initial cracks can also arise during the curing processes of the epoxy adhesive because of shrinkage and have also been observed in experimental settings where hard surfaces were attached to each other by polyurethane and brittle

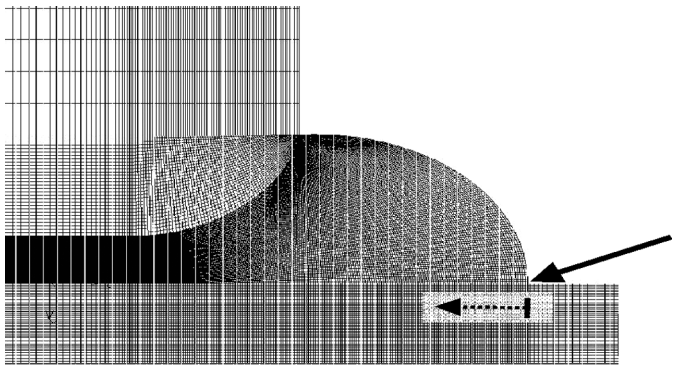

FIGURE 5 Enlarged part of the adaptive FE mesh at the edge of the adhesive with the assumed location of debonding initiation (solid arrow).

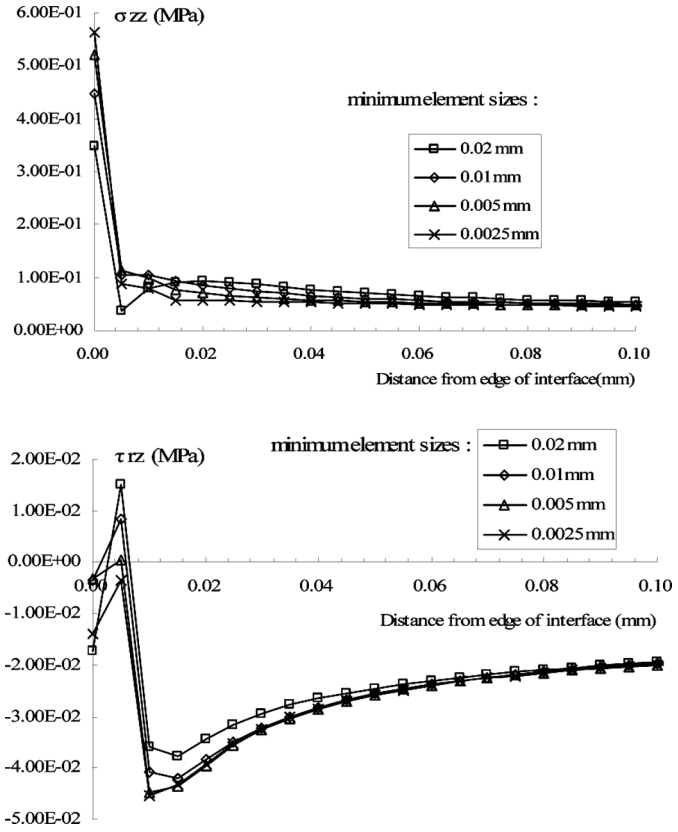

FIGURE 6 Projected FE results of σ_{zz} (left) and τ_{rz} (right) in the interface layer with different minimal element sizes.

epoxies [8]. The bonding of the epoxy on the silicone rubber cannot be assumed to be perfect because microvoids (see, *e.g.*, Ref. [15]) are known to be present between the silicone coating and epoxy glue. In Figure 8, the thickness dependence of the energy-release rate, G_0, at $\sigma_o = 0.1\,\text{MPa}$ with respect to various crack lengths is shown. In accordance with intuitive physical understanding, G_0 increases with the crack length. The characteristics of the G_0 *versus* t relation, however, are essentially the same for the different crack lengths—G_0 is relatively small for thin coatings and increases with the coating thickness. Similar results have been determined in Ref. [8] where the debonding of Plexiglas® and steel surfaces attached to each other by adhesives has been analyzed with respect to the thickness of the adhesive layer. Therein, the critical energy-release rate was reported to increase with

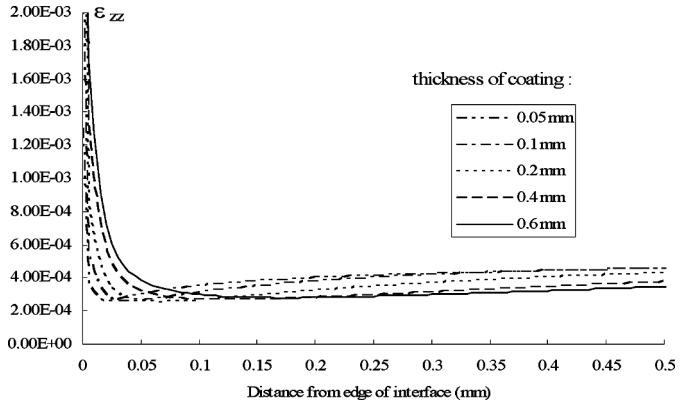

FIGURE 7 ε_{zz} in the interface for various coating thicknesses.

the initial crack length, and bonding strength increased for decreasing adhesive thickness as in Ref. [9] for a different experimental setting and materials.

As the Young's modulus, E, of the different silicone coatings applied in the experiments differs quite strongly, additional simulations have been performed for different values of E. In Figure 9, G_0 versus t curves for different E values have been plotted. Similar to the behavior in Figure 8, G_0 decreases with increasing E. In both cases—decreasing thickness and increasing E—the material system is stiffened, which correlates to smaller G_0 values.

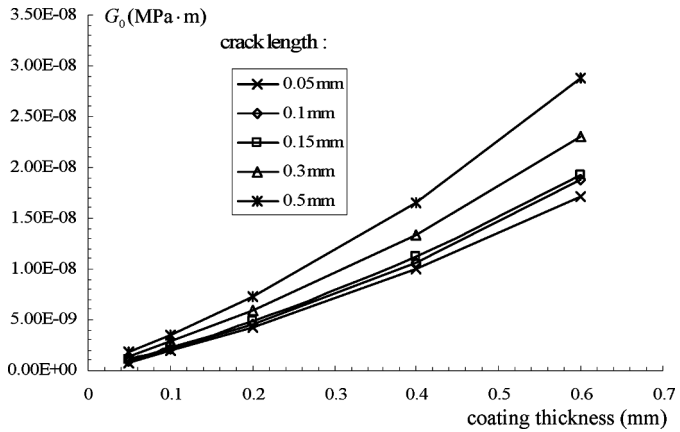

FIGURE 8 Coating thicknesses t versus G_0 for various initial crack lengths and $\sigma_o = 0.1\,\text{Mpa}$.

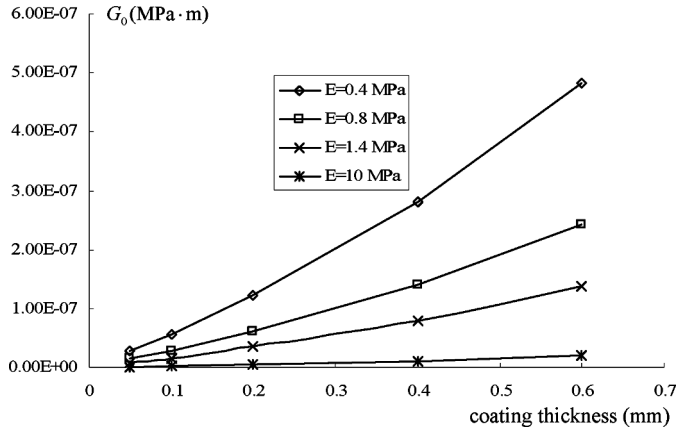

FIGURE 9 Coating thicknesses t versus G_0 for different elastic moduli, E, and $\sigma_o = 0.1\,\text{Mpa}$.

ANALYSIS AND DISCUSSION

The relation between the experimentally determined pull-off forces *versus* coating thickness shown in Figure 3 and the coating-thickness dependence on the energy-release rate in Figures 8 and 9 are discussed in this section. A common debonding criterion based on the energy-release rate G can be stated as (see, *e.g.*, Ref. [16])

$$G = G_{crit}, \tag{4}$$

where the critical energy-release rate, G_{crit}, is basically a material parameter characterizing the interface properties, depending on the interaction, bonding energies, and microvoid densities.

Generally, the stress-intensity factors K_I, K_{II}, and K_{III} are proportional to the applied stress fields, which is also true for bimaterials considered here (see, *e.g.*, Ref. [17] for more details). As the energy-release rate G is in turn proportional to $K_I^2,\ K_{II}^2,$ and K_{III}^2, the energy-release rate is proportional to the square of the applied stress, *i.e.*,

$$G \propto \sigma^2. \tag{5}$$

The energy-release rates determined by the FE simulations (Figures 8 and 9), on the other hand, are performed for a constant applied stress, σ_o, and show a significant dependence on the thickness, t, which yields the proportionality

$$G_o(t) = G(\sigma_o, t) \propto f(t). \tag{6}$$

Combining Eqs. (5) and (6) yields

$$G \propto f(t)\sigma^2, \qquad \text{or equivalently, } G = cG_o(t)\frac{\sigma^2}{\sigma_o^2}, \tag{7}$$

where c is a dimensionless constant (obeying the relation $c \propto 1/E$; see, *e.g.*, Ref. [17]) characterizing the proportionality of G and σ^2. The debonding criterion (4) $G = G_{crit}$ then yields

$$\sigma_{crit} = \sigma_o \sqrt{\frac{G_{crit}}{c\ G_o(t)}},$$

and therefore the critical stress at which debonding occurs is proportional to $1/\sqrt{G_o(t)}$; thus

$$\sigma_{crit}(t) \propto \frac{1}{\sqrt{G_o(t)}}. \tag{8}$$

Besides a prefactor c_2 in the order of $c_2 \approx \sigma_o\sqrt{G_{crit}/c}$, this relation should have the same characteristics as $\sigma_{crit}(t)$. In Figure 10, $1/\sqrt{G_o(t)}$ *versus* thickness is shown for various crack lengths with very similar characteristics to the fitted curves of the experiments in Figure 3. A fit of the FE simulation data *via* $y = at^{-b}$ for thicknesses between 0.05 mm and 0.6 mm results in similar exponents as those obtained in Figure 10. The exponent b, ranging between 0.550 and 0.634, decreases with increasing initial crack length.

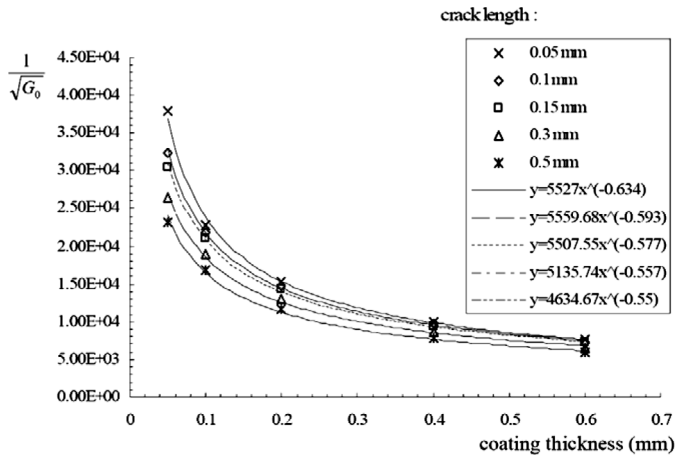

FIGURE 10 Coating thickness versus $1/\sqrt{G_0}$ for different initial crack lengths.

From these considerations, the proportionality $\sigma_{crit} \propto \sqrt{E}$ can be deduced as $\sigma_{crit} = \sigma_o \sqrt{G_{crit}/cG_e(t)}$ where $G_{crit} = \text{const.}$ and $c \propto 1/E$. Accordingly, the exponent b hardly changes when varying the Young's modulus (Figure 11). The exponents b from the fitted curves of the simulations (Figures 10 and 11) are $b = 0.550$ to 0.634 in the range of the values obtained from fitting of the experimental data ($b = 0.483$, 0.867). To a certain extent, the wider range of b in the experimental data may be viewed as the result of the experimental scatter (see Figure 3). In the variations of the properties, only the initial crack length affects the exponent b to appreciable extents. Note that the critical energy-release rate, G_{crit}, characterizing the bonding strength in this problem should also only influence the prefactor a in the fit $y = at^{-b}$. However, there may, also be other sources in the debonding process that have not been taken into account in our simulation model that may also influence the exponent b.

The adhesive bonding is usually not perfect. Similar to the roughness of surfaces, the interface morphology may also be considered to have fractal properties where related wavelengths range from the macroscopic to nanometer scales. In most cases there are voids associated with different length scale ranges [18] in the adhesive–substrate interface, and because of these microvoids, the material interface may have to be viewed as a somehow damaged region. Besides, because of the fabrication process, the morphology over the whole interface may not be consistent as, at the center, the adhesive may be subjected to hardly any material flow in the wetting stage.

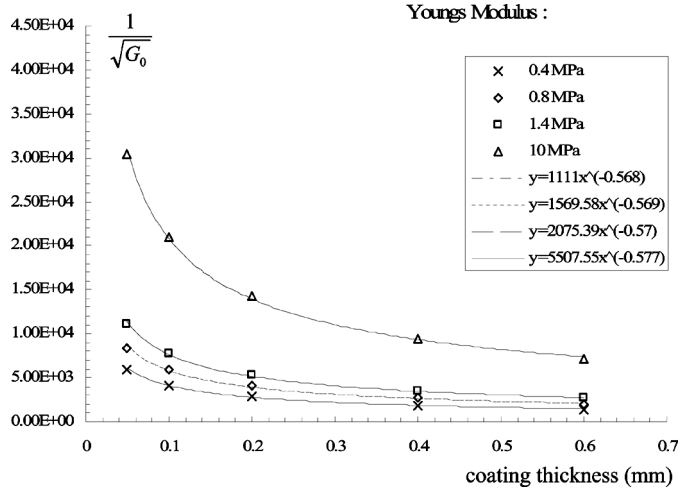

FIGURE 11 Coating thickness versus $1/\sqrt{G_0}$ for different Young's moduli.

The initial geometry (*i.e.*, particularly the crack length) of both materials is not the same in spite of the fact that the samples of both materials have been fabricated in essentially the same way. If an initial crack is assumed to be present, as in our simulations, the results presented in Figure 11 show that the exponent b is strongly dependent on the initial crack length. The initial crack length will, however, be dependent on the compliance of the material and the difference in the adhesive forces between the two materials in form of, *e.g.*, van der Waals forces. With increased compliance as a consequence of a smaller E, adhesive forces may reduce the initial crack length of soft materials more than in stiffer materials with higher E. The adhesive forces in the material interface have a similar effect on the initial crack length. If strong adhesive forces would be present, it is more likely that cracks (which may open during handling of the samples) are smaller prior to testing. The decrease in the initial crack length will in turn increase the exponent b as illustrated in Figure 11. Because the chemical components of the materials are different, the adhesive forces between the silicone rubber and the epoxy glue may also be different, which results in a different initial crack length. The SC6 coating, for instance, is comparable with almost pure silicone, and therefore only bonding *via* van der Waals forces can be assumed, whereas the more complex molecular structure of the SP1 coating may also enable chemical bonds with epoxy molecules, which would increase the bonding forces significantly.

In this respect, it should also be noted that, because of the softness and visco-elastic behavior of the silicone, cracks that may have arisen during handling may also close to a certain extent because of adhesional van der Waals forces. Generally, the actual microscopic area of contact between the material interfaces will, decrease as the epoxy adhesive in the cured condition will not be as compliant as in the wetting stage. A determination of the actual area of contact up to now cannot be properly measured nor controlled [19]. This perspective may also motivate the viewpoint that the initial crack lengths are actually effective crack lengths, as our macroscopic model does not take the surface morphology explicitly into account.

Assuming that the differences in the exponent b merely arise because of the initial crack length, a comparison of the fitted exponents of the experimental and simulation data would indicate that the initial cracks in the pull-off tests with the SP1 coating are actually smaller than 0.05 mm. Although the application of a linear elastic analysis with the virtual crack closure technique may be considered to be a good first-order approximation of this problem, it should be observed that the exponents of the simulation data do not decrease

significantly at about $b = 0.55$ for initial crack lengths larger than 0.3 mm (see Figure 10). Therefore, the experimental values for $b = 0.4833$ are difficult to obtain by varying the initial crack length. This yields the conclusion that either the experimental data may not be representative or that other mechanisms are present that are not contained in the linear elastic simulation. Considering the scatter in the experimental data a direct comparison may be misleading, however.

One may argue that the rather moderate differences may have their origin in the nonlinear material behavior not reflected in the simulations. For the observed debonding stresses, the strains are rather small (Figure 7), and therefore nonlinearity should not be pronounced. Also, micromechanically local stress/strain concentrations due to asperities seem unlikely because the roughness of the cured silicone coatings measured by atomic force microscopy (AFM) is very low, with an average roughness less than a few nanometers.

As observed for other material interfaces (*e.g.*, Ref. [20]), the debonding criterion [Eq. (4)] may be influenced by mode mixity, and therefore the debonding criterion may be dependent on a relation between G_I and G_{II}, which can be described by the phase angle $\Psi = \arctan(\sqrt{G_I/G_{II}})$. The change of the phase angle has been plotted in Figure 12 and exhibits an increase with decreasing coating thickness. Thus, the thicker

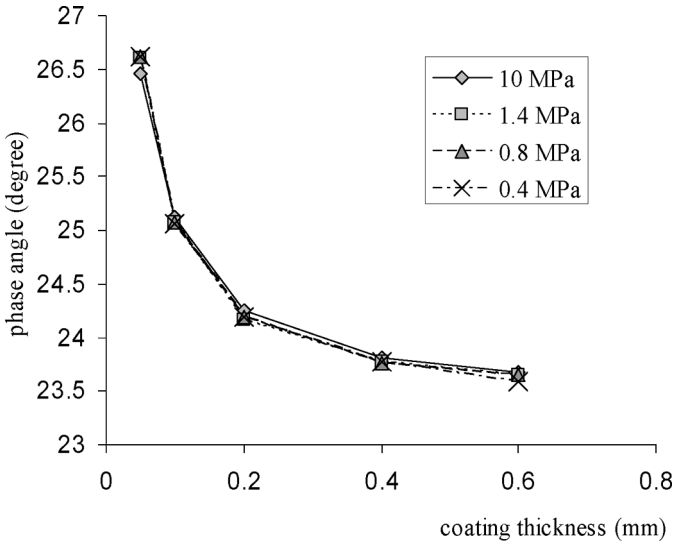

FIGURE 12 Coating thickness versus phase angle $\Psi = \arctan(\sqrt{G_I/G_{II}})$ for different Young's moduli.

the coating layer, the smaller the portion of mode II component in the total energy-release rate. In general, debonding under mode I (opening mode) will require smaller forces than under mode II (shear mode). Therefore, the change in the phase angle may be associated with the change of the exponent b. However, neither Young's modulus (see Figure 12) nor initial crack length (not shown here) seem to affect this dependency appreciably.

Another source may be because the process zone of debonding is very small, and therefore size-dependent, nonlocal effects may play a role. Such nonlocal effects at the micron and submicron length scale have been observed in microbeam bending [21,22] and indentation experiments [23–25], and these experiments indicate that silicone rubber has a particularly strong size-dependent behavior that may be different in both materials. The size-dependent deformation on the micron- and nanoscale is usually described by strain or rotational gradients, which are also present in the debonding process zone. For metals, nonlocal effects in the debonding process have been discussed in Refs. [26,27]. Recent experiments of glass particles in an epoxy matrix also indicate that size effects are also present in the debonding process of polymeric materials [28].

Lastly, it should be mentioned that we have assumed that the geometry of the epoxy layer is the same for all pull-off test samples. This may not be true because (i) the different coatings as the adhesive forces between coating and epoxy glue may be different during the hardening and curing process and (ii) the geometry of the epoxy glue may also be different for different coating thicknesses as thicker coatings will be essentially more compliant and therefore may result in a different distribution of the coating than in thinner coatings.

CONCLUSIONS

The pull-off tests have been analyzed with the FE method, applying the virtual crack closure technique. The simulations illustrate the influence of the elastic modulus and the initial crack lengths on the thickness-dependent pull-off forces. The analysis of these simulations indicates that the pull-off forces are approximately proportional to the elastic modulus and the critical energy-release rate and that the fit of the debonding stress by $y = at^{-b}$ yields a very good approximation. Whereas elastic modulus and critical release rate should be proportional to the fit variable a, the analysis indicates that initial crack length changes the exponent b in the $y = at^{-b}$ fit and therefore alters the characteristics of the thickness dependence of the pull-off forces. Both elastic modulus and adhesive forces, which are represented in

our analysis by the critical energy-release rate, may have an indirect influence on the initial crack length. Although the simulations are in reasonably good agreement with the experiments, other deformation mechanisms may also be present that are not reflected in our model.

ACKNOWLEDGMENTS

The support of this work by the North Dakota Experimental Program to Stimulate Competitive Research (EPSCoR Program) (EPS-0447679) and the Office of Naval Research (Grant N00014-04-1-0597) is highly appreciated.

REFERENCES

[1] Shull, K. R., Ahn, D., Chen, W.-L., Flanigan, C. M., and Crosby, A. J., *Macromol. Chem. Phys.* **199**, 489–511 (1998).
[2] Shull, K. R. and Creton, C., *J. Polym. Sci. B* **42**, 4023–4043 (2004).
[3] Chung, J. Y. and Chaudhury, M. K., *J. Adhes.* **81**, 1119–1145 (2005).
[4] Webber, R. E., Shull, K. R., Roos, A., and Creton, C., *Phys. Rev. E* **68**, 021805 (2003).
[5] Ganghoffer, J. F. and Schultz, J., *J. Adhes.* **55**, 285–302 (1996).
[6] Teng, J. G., Zhang, J. W., and Smith, S. T., *Constr. Build. Mater.* **16**, 1–14 (2002).
[7] Anderson, G. P., DeVries, K. L., and Williams, M. L., *Int. J. Frac.* **9**, 421–435 (1973).
[8] Anderson, G. P. and DeVries, K. L., *Int. J. Frac.* **39**, 191–200 (1989).
[9] Bascom, W. D. and Cottington, R. L., *J. Adhes.* **7**, 333–346 (1976).
[10] Reedy Jr., E. D. and Guess, T. R., *Int. J. Sol. Struc.* **39**, 325–340 (2002).
[11] Reedy Jr., E. D., *J. Mater. Res.* **21**, 2660–2668 (2006).
[12] Krueger, R., *Appl. Mech. Rev.* **57**, 109–143 (2004).
[13] Sun, Z., Wan, K.-T., and Dillard, D. A., *Int. J. Sol. Struc.* **41**, 717–730 (2004).
[14] Cook, R. D., Malkus, D. S., Plesha, M. E., and Witt, R. J., *Concepts and Applications of Finite Element Analysis*, 4th ed. (J. Wiley & Sons, New York, 2002).
[15] Yang, C., Tartaglinoa, U., and Persson, B. N. J., *Eur. Phys. J. E* **19**, 47–58 (2006).
[16] Lemaitre, J. and Chaboche, J.-L., *Mechanics of Solid Materials* (Cambridge University Press, Cambridge, 1990).
[17] Hwu, C., *Eng. Frac. Mech.* **3**, 89–97 (1993).
[18] Persson, B. N. J., *Surface Science Reports* **61**, 201–227 (2006).
[19] Kalnins, M., Sirmacs, A., and Malers, L., *Int. J. Adhesion Adhesives* **17**, 365–372 (1997).
[20] Evans, A. G., Ruehle, M., Dalgleish, B. J., and Charalambides, P. G., *Metallurgical Transactions A* **21**, 2419–2429 (1990).
[21] Lam, D. C. C., Yang, F., Chong, A. C. M., Wang, J., and Tong, P., *J. Mech. Phys. Sol.* **51**, 1477–1508 (2003).
[22] McFarland, A. W. and Colton, J. S., *J. Microm. Microeng.* **15**, 1060–1067 (2005).
[23] Zhang, T.-Y. and Xu, W.-H., *J. Mater. Res.* **17**, 1715–1720 (2002).
[24] Nikolov, S., Han, C.-S., and Raabe, D., *Int. J. Sol. Struc.* **44**, 1582–1592 (2007).
[25] Han, C.-S. and Nikolov, S., *J. Mat. Sci.* **22**, 1662–1672 (2007).
[26] Wei, Y. and Hutchinson, J.W., *J. Mech. Phys. Sol.* **45**, 1137–1159 (1997).
[27] Evans, A. G., Hutchinson, J. W., and Wei, Y., *Acta Materialia* **47**, 4093–4113 (1999).
[28] Agde Tjernlund, J., Gamstedt, E. K., and Gudmundson, P., *Int. J. Sol. Struc.* **43**, 7337–7357 (2006).